



HAL
open science

Transient response of a rotor-AMBs system connected by a flexible mechanical coupling

Slim Bouaziz, Najib Belhadj Messaoud, Jean-Yves Choley, Mohamed Maatar,
Mohamed Haddar

► **To cite this version:**

Slim Bouaziz, Najib Belhadj Messaoud, Jean-Yves Choley, Mohamed Maatar, Mohamed Haddar.
Transient response of a rotor-AMBs system connected by a flexible mechanical coupling. *Mechatronics*,
2013, 23 (6), pp.573-580. 10.1016/j.mechatronics.2013.05.002 . hal-01911013

HAL Id: hal-01911013

<https://hal.science/hal-01911013>

Submitted on 8 Jun 2023

HAL is a multi-disciplinary open access archive for the deposit and dissemination of scientific research documents, whether they are published or not. The documents may come from teaching and research institutions in France or abroad, or from public or private research centers.

L'archive ouverte pluridisciplinaire **HAL**, est destinée au dépôt et à la diffusion de documents scientifiques de niveau recherche, publiés ou non, émanant des établissements d'enseignement et de recherche français ou étrangers, des laboratoires publics ou privés.

Transient response of a rotor-AMBs system connected by a flexible mechanical coupling

Slim Bouaziz ^{a,*}, Najib Belhadj Messaoud ^a, Jean-Yves Choley ^b, Mohamed Maatar ^a, Mohamed Haddar ^c

^aDynamic Mechanical Systems Unit (UDSM), National School of Engineers of Sfax (ENIS), University of Sfax, BP.1173, Sfax 3038, Tunisia

^bLaboratory of Engineering in Mechanical Systems and Materials, SUPMECA, Saint-Ouen, France

^cMechanics Modeling and Production Unit (U2MP), National School of Engineers of Sfax (ENIS), University of Sfax, BP.1173, Sfax 3038, Tunisia

In this paper, the effect of angular misalignment on the transient dynamics of a rotor-Active Magnetic Bearings (AMBs) system was examined with numerical analysis. A spatial model of a misaligned rotor mounted in two identical AMBs is setup to account angular misalignment with a flexible coupling having torsional and lateral flexibility. The driving rotor was powered by an electric motor in transient regime. Three models of AMBs were used with four; six and eight magnets. They were powered by bias and con-trol current. The AMBs dynamics support parameters were modeled by stiffness and damping matrices. These were computed through an electromagnetic theory and derivation of the magnetic forces. The gen-eral equations of motion of the driven rotor were derived and solved using the Newmark time integration method. Simulation results were carried out to determine the frequency and transient responses in term of misalignment magnitude. Dynamic responses come to confirm a significant influence of the transient regime on the dynamic behavior of misaligned rotor. Simulated results also reveal that vibrations induced by angular misalignment were more important in the case of AMBs with four magnets. Spectral compo-nents of the system response were investigated, in sort to present diagnostic information about the sig-nature of this kind of fault in transient regime.

1. Introduction

During the past two decades a diversity of AMBs studies have been done. The part of AMBs technology has been recently intensively developed because the non-contact support, absence of lubrication system, friction free rotation and potential aptitude at high temperature and higher rotating speed. In rotating machines, misalignment is one of the mainly common observed faults. However, there have been some researches to know its effect on overall dynamics of the rotor system. For understanding the dynamics of misaligned rotors and reducing the ambiguity so as to improve the reliability of the misalignment fault diagnosis, Patel and Darpe [1] presented an experimental investigation of the vibration response of misaligned coupled rotors supported on rolling element bearings to evaluate the influence of misalignment and its type on the forcing characteristics of a flexible coupling. The means of reacting to applied loads, such as inertia, maneuver or unbalance, have been compared with rolling element, hydrodynamics and elasto-hydrodynamic bearings by Bouaziz et al. [2] and Attia Hili et al. [3]. Bouaziz et al. [4] investigated the dynamic response of a rigid misaligned rotor mounted in two identical AMBs. Three

simplified models of radial AMBs are presented, where four, six and eight magnets are powered by a bias current. It is shown that angular misalignment is such that the $2\times$ and $4\times$ running speed components are predominant. Their magnitudes differ with the number of magnets in the bearing. Belhadj Messaoud et al. [5] are studied dynamic behavior of AMBs in presence of angular misalignment defect. A variable and adaptable stiffness dynamic absorber is used by Wang and Lai [6] to control the vibration of parametrically excited beam. Mohamed and Emad [7] investigated effects of the gyroscopic motion on nonlinear oscillations of the magnetic bearing system and establish that the hopf bifurcation occur approximately certain critical speeds. Attia Hili et al. [8] investigated the response of a flexible rotor-bearing system with unbalanced disk. Lees [9] studied the effect of misalignment in rigidly coupled rotors. For the case of parallel misalignment, the kinematics of the relating bolts was proposed. Expressions for phase and amplitude of the vibration response were presented, which shows excitation to expand at double the rotor speed owing to misalignment. Dewell and Mitchell [10] gave a discussion of the harmonics arising in flexible couplings. Gibbons [11] was the primary deriving the misalignment reaction forces generated in different types of couplings. The effect of coupling misalignment on vibration response of the rotor was numerically evaluated by Sekhar and Prabhu [12]. They recommended $2\times$ vibration response

* Corresponding author. Tel.: +216 74 274 088; fax: +216 74 275 595.
E-mail address: slim.bouaziz1@gmail.com (S. Bouaziz).

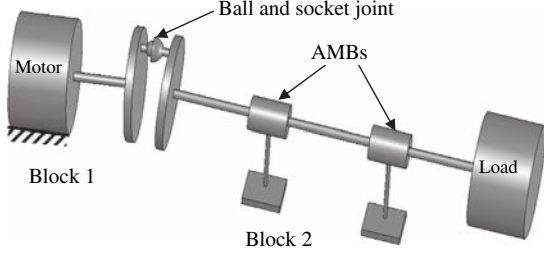


Fig. 1. Model describing the misalignment.

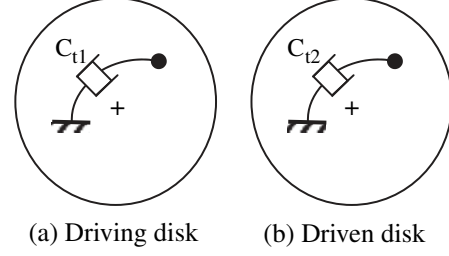


Fig. 3. Damping modeling of a pair of disk coupling.

as characteristic signature of misaligned shafts. A model for the flexible coupling-rotor-ball bearing system was derived by Lee and Lee [13]. From orbital analysis, anisotropy of bearing stiffness was recommended as the misalignment indicator. The other approach habitually used to simulate misalignment effect in rotor system was from kinematics of the couplings. In a pair of papers, Xu and Marangoni [14,15] gave an analysis of a system counting a flexible coupling and backed up their predictions with laboratory experiments. It concluded that the source of the great harmonic components in the vibration signal caused by the nonlinear behavior of the flexible coupling, a systematic attempt to model the misalignment effect analytically by the universal joint kinematics was made. Al-Hussain and Redmond [16] modeled a flexible coupling in the form of a radial rigid, pinned joint with rotational stiffness. Bahaloo et al. [17] studied velocity transients of a misaligned rotor with a simplified model. On the contrary, the model presented henceforth by the authors was appropriated to investigate the behavior of existent rotating machinery, in view of all the possible features. The results obtained by Zhang and Zu [18] indicate that the rotor-AMBs system with eight magnets and time-varying stiffness was able of auto-controlling transient condition chaos to steady state periodic and quasi periodic motions.

The present study outlines a method of determination of the misalignment excitation, wherein a coupled rotor bearing system with ball and socket flexible coupling is investigated on transient regime. The influence of the angle of misalignment and the number of magnets by bearings on the rotor dynamic behavior is presented. The work starts by developing the equation of motions of two rotors whose axis of rotation is offset due to pure angular misalignment. The equations of motions are solved numerically to study the general effect of misalignment on the time and frequencies responses. This paper is an extension of the research works published by Bouaziz et al. [4] on 2011. The technical contribution of the present investigation is to study the dynamic behavior of misaligned rotors in non-stationary conditions and taking into

account the torsional rigidity of the shafts, the damping of coupling and the dynamics of AMBs.

2. Model of a misaligned rotor

We consider, in Figs. 1 and 2, a theoretical model that describes the spatial angular misalignment defect. The model assumptions are the following: It is divided into two main blocks.

Block 1 includes the driving motor and the first disk of flexible coupling connected by shaft 1. Block 2 includes the second disk of flexible coupling and the load connected by shaft 2; it is supported by two AMBs (4) and (5). The different parameters of the studied model are shown in Fig. 2. A driving torque C_m is applied on the coupling loaded by a torque C_r . θ_{ij} and J_{ij} are respectively the angular displacement and the moment of inertia of the component j in the block i ($i, j = 1, 2$). We consider that block 1 and block 2 have the same weight m . The damping coefficients in the coupling are shown in Fig. 3. The two shafts have a fault alignment of an angle $\alpha_i + \alpha(t)$ in (x, y) plane and $\beta(t)$ in (x, z) plane, as shown in Fig. 4, α_i is an imposed angle.

3. Formulation of the governing equations

3.1. Modeling of AMBs

The typical geometric parameters of magnets used in AMBs are presented in Fig. 5. It is assumed that every magnet have identical structure. For simplicity, the fringe magnetic flux, the eddy current loss, the saturation and hysteresis of the magnetic core material, the magnetic flux leakage and the coupling effects between magnets are ignored. Three simplified models of current AMB are considered in the present study, where four, six and eight magnets are symmetrically located and powered by the bias current I_0 and control current $\pm I_i$ ($i = 1, 2, 3, 4$). The electromagnetic forces produced by every opposed pair of magnet can be expressed as [4]:

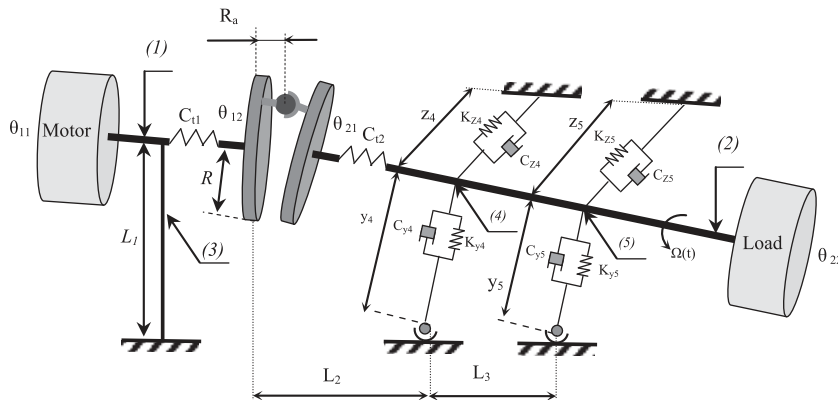


Fig. 2. Model of angular misalignment with coordinates systems.

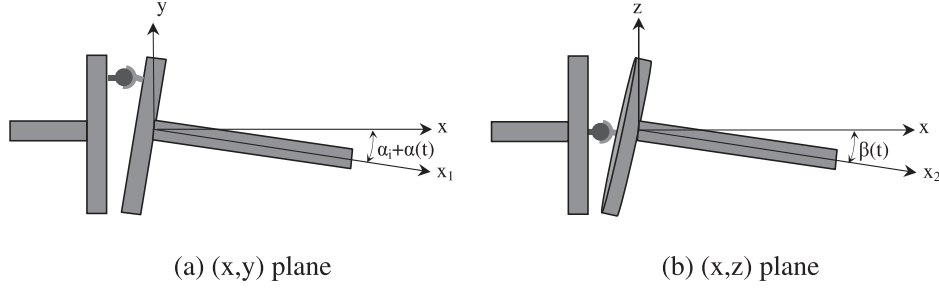


Fig. 4. The angular misalignment of coupled rotors.

$$F_i(I_i, \delta_i) = -\frac{A\mu_0 N^2}{4} \left[\left(\frac{I_0 + I_i}{C_0 + \delta_i} \right)^2 - \left(\frac{I_0 - I_i}{C_0 - \delta_i} \right)^2 \right] \cos\theta, i$$

$$= 1, 2, 3, 4 \quad (1)$$

where μ_0 is the permeability of a vacuum, A is the cross-section area of one electromagnet, N is the number of windings in each magnet coil, C_0 is the air gap between the stator and shaft, I_0 represents the bias current which plays a role of producing electromagnetic field, I_i ($i = 2, 3, 4$) is the control current in the i direction, $I_1 = i_1$, $I_i = i_0 + i_i$, i_0 is the static component of the control current relative to the weight of the rotor, i_i ($i = 1, 2, 3, 4$) is the feedback part of the control current and δ_i ($i = 1, 2, 3, 4$) represents the displacements of the rotor in the i th direction.

Taking into consideration the current Proportional-Derivative (PD) controller in the rotor-AMBs system, the feedback components of the control current (i_i) can be written [4]:

$$i_i = k_p \delta_i + k_d \dot{\delta}_i \quad (2)$$

where k_p and k_d respectively represent the proportional and the derivative gains and $\dot{\delta}_i$ is the velocity in the i th direction and φ_i is the angle between the first and the i th magnet ($i = 1, 2, 3, 4$). The displacements of the rotor in the i th direction δ_i can be expressed as [4]:

$$\delta_i = y \cos \varphi_i + z \sin \varphi_i (i = 1, 2, 3, 4) \quad (3)$$

We can deduct the expression of the resultants electromagnetic forces F_y and F_z in, respectively, the horizontal and vertical directions. It has the following form:

$$\begin{cases} F_y = \sum_{i=1}^4 F_i \cos \varphi_i \\ F_z = \sum_{i=1}^4 F_i \sin \varphi_i \end{cases} \quad (4)$$

The electromagnetic forces of AMB with four, six and eight magnets are presented in the Appendix.

The classic linearized model with eight stiffness and damping coefficients is employed for the bearing modeling in the present work. In this model, the forces at each bearing are assumed to obey the governing equations of the following form [2,5]:

$$[K_{ij}] \begin{Bmatrix} y \\ z \end{Bmatrix} + [C_{ij}] \begin{Bmatrix} \dot{y} \\ \dot{z} \end{Bmatrix} = \begin{Bmatrix} F_y \\ F_z \end{Bmatrix} \quad (5)$$

where y and z are the AMB degrees of freedom, $[K_{ij}]$ and $[C_{ij}]$ are respectively the bearing stiffness and damping matrices. They are expressed by:

$$\begin{cases} [K_{ij}] = \begin{bmatrix} K_{yy} & K_{yz} \\ K_{zy} & K_{zz} \end{bmatrix} \\ [C_{ij}] = \begin{bmatrix} C_{yy} & C_{yz} \\ C_{zy} & C_{zz} \end{bmatrix} \end{cases} \quad (6)$$

3.2. Modeling of electric motor

Using the kinetic energy theorem and neglecting the power losses, the rotational velocity of an electric motor can be related to the driven torque and to the receiver torque by [19]:

$$J \frac{d\Omega}{dt} = C_m - C_r \quad (7)$$

where J is the correspondent moment of inertia of the rotating parts.

The relation between speed of the motor and driving torque is expressed by [19]:

$$C_m = \frac{T_b}{(1 + (s_b - s)^2)((a/s) - bs^2)} \quad (8)$$

where s_b and T_b are the slip and torque at breakdown, respectively, a and b are all constant properties of the motor, presented in Table 2, and s is the proportional drop in speed given by [20]:

$$s = 1 - \frac{N}{N_s} \quad (9)$$

N is the definite rotational speed of the motor and N_s is the synchronous speed. Load torque (C_r) characteristic is chosen proportional to the square of the rotational speed. This is the case for some number of receivers such as pumps [19]:

$$C_r = h\Omega^2 \quad (10)$$

where h is a coefficient depending on the driven system characteristics.

Eq. (7) is transformed into the subsequent differential equation:

$$\frac{d\Omega}{dt} = \frac{1}{J} (C_m(\Omega, t) - C_r(\Omega, t)) \quad (11)$$

3.3. Energy equations of the receptor shaft

The equations of motion for a studying model can be derived using the ten generalized coordinate vector of the degrees of freedom θ_{11} , θ_{12} , y_4 , z_4 , y_5 , z_5 , θ_{21} , θ_{22} , α and β .

$$\{q\} = [\theta_{11} \ \theta_{12} \ y_4 \ z_4 \ y_5 \ z_5 \ \theta_{21} \ \theta_{22} \ \alpha \ \beta]^T \quad (12)$$

The potential energy of the system can be written as:

$$E_p = \frac{1}{2} [k_{y_4} y_4^2 + k_{z_4} z_4^2 + k_{y_5} y_5^2 + k_{z_5} z_5^2 + k_{\theta_1} (\theta_{11} - \theta_{12})^2 + k_{\theta_2} (\theta_{21} - \theta_{22})^2] \quad (13)$$

Rayleigh's dissipation function due to the bearings and coupling damping is given by:

Table 1
System parameters.

Parameter	Symbol	Value	Unit
Permeability of a vacuum	μ_0	$4\pi \times 10^{-7}$	Wb/Am
Air gap between the stator and the shaft	C_0	1.5	mm
Effective cross-sectional area	A	200	mm ²
Number of windings around the core	N	300	-
half angle of the radial electromagnetic	θ	22.5	degree
Bias current	I_0	3	A
Static component of the control current	i_0	0.5	A
Rotor length	L	550	mm
Height of bearings motor shaft	L_1	25	mm
Distances between the motor shaft and bearing (4)	L_2	80	mm
Distance between bearings (4) and (5)	L_3	400	mm
Stiffness coefficients	$K_{ij}(i, j = x, y)$	-	N/m
Damping coefficients	$C_{ij}(i, j = x, y)$	-	N s/m
Disk radius	R	80	mm
Moment of inertia	I	0.136	kg m ²
Coupling radius	R_a	2	mm
Rotor mass	m	1.34	kg
Angle of misalignment	α_i	-	-

Table 2
Motor characteristics.

Motor type	ABB-MT 90L
Electrical specifications	4 poles, 50 Hz 3 phases, 415 V
Yield power (kW)	1.5
Full load speed (rpm)	1420
Slip s_b	0.315
Motor constant a	1.711
Motor constant b	1.316

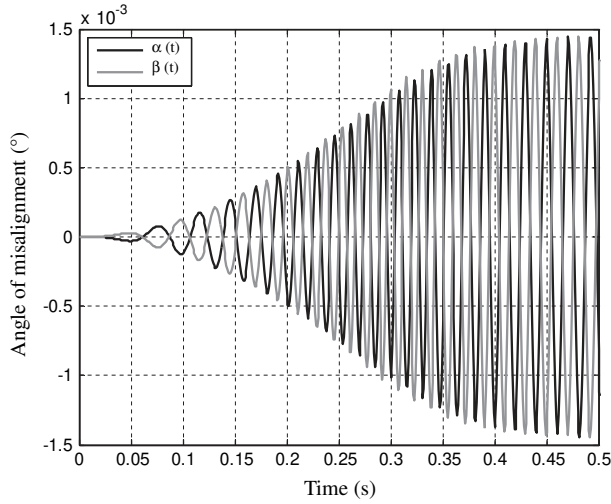


Fig. 6. Angular misalignment of the misaligned rotor, $\alpha_i=0^\circ$.

where

$$C_{11} = -2mR^2\Omega \cos(\Omega t) \sin(\Omega t) + C_{yy}[(B^2 + D^2) \cos^2 \alpha_i + 2A^2 \times \sin^2 \alpha_i - 2A \cos \alpha_i \sin \alpha_i (B + D)] \quad (28)$$

$$C_{22} = 2mR^2\Omega [\sin^2(\Omega t) \cos \alpha_i + \cos^2(\Omega t)] + \frac{1}{2}B(C_{yz} + C_{zy}) \times (B \cos \alpha_i - A \sin \alpha_i) + \frac{1}{2}D(C_{yz} + C_{zy})(D \cos \alpha_i - A \sin \alpha_i) \quad (29)$$

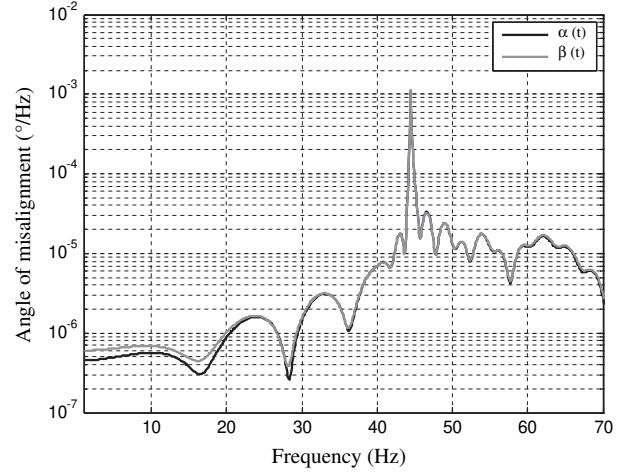


Fig. 7. Frequency spectrum of the misaligned rotor, $\alpha_i=0^\circ$.

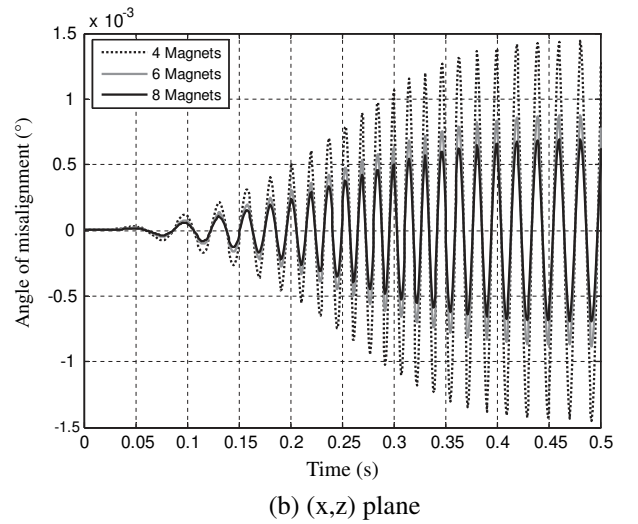
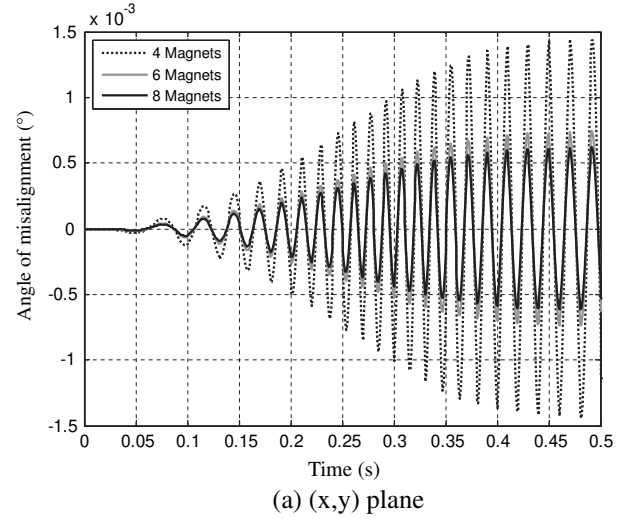


Fig. 8. Angular misalignment of the misaligned rotor, $\alpha_i=0^\circ$.

$$C_{33} = -2mR^2\Omega \sin^2(\Omega t) + B(C_{yz} + C_{zy})(B \cos \alpha_i - A \sin \alpha_i) + D(C_{yz} + C_{zy})(D \cos \alpha_i - A \sin \alpha_i) \quad (30)$$

$$C_{44} = mR^2\Omega \sin(\Omega t) \cos(\Omega t) + C_{zz}(B^2 + D^2) \quad (31)$$

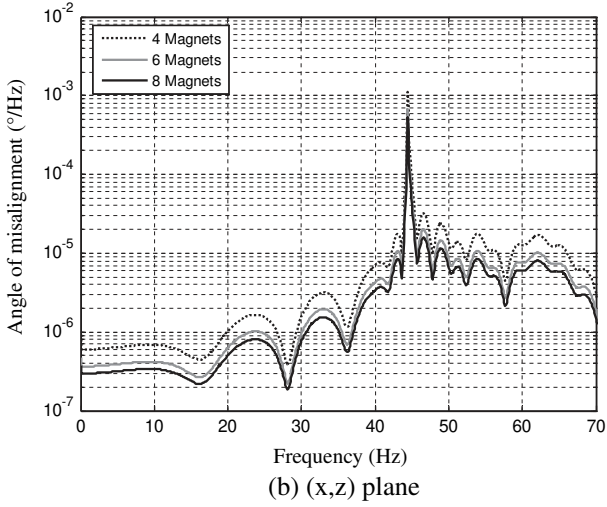
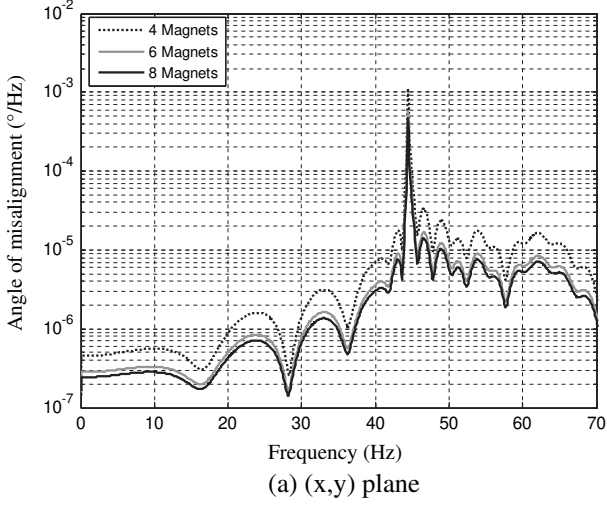


Fig. 9. Frequency spectrum of the misaligned rotor, $\alpha_i=0^\circ$.

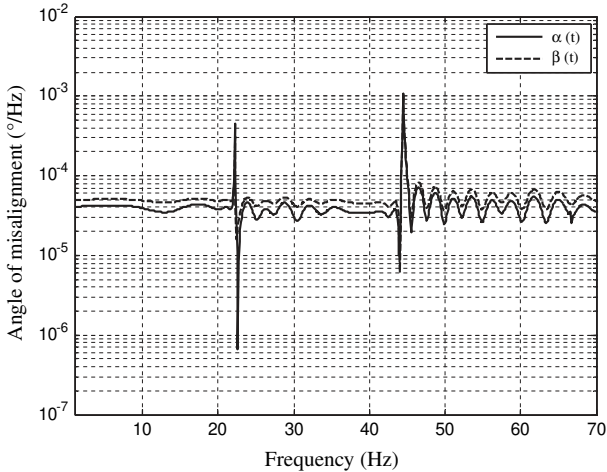


Fig. 10. Frequency spectrum of the misaligned rotor, (x,y) plane, $\alpha_i=0.1^\circ$.

with,

$$A = L_1 + R \cos(\Omega t), B = L_2 - R_a, D = L_2 - R_a + L_3 \text{ and} \\ E = \frac{L}{2} + R_a \quad (32)$$

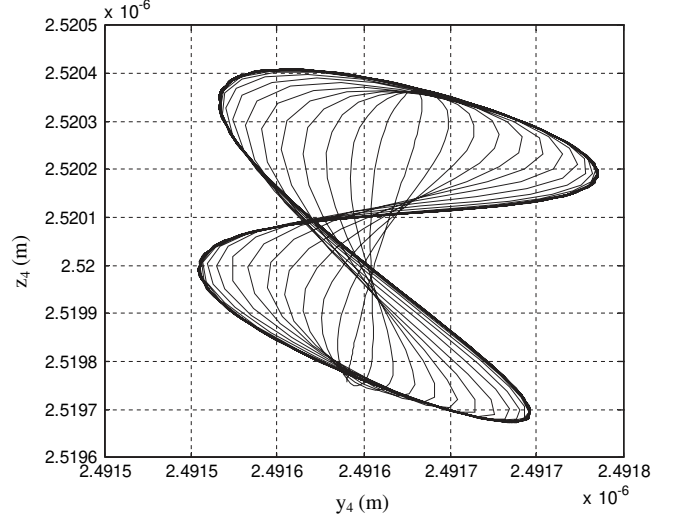


Fig. 11. Orbit plot of vibration response of the misaligned rotor in bearing 4, $\alpha_i=0.1^\circ$, AMBs with 6 magnets.

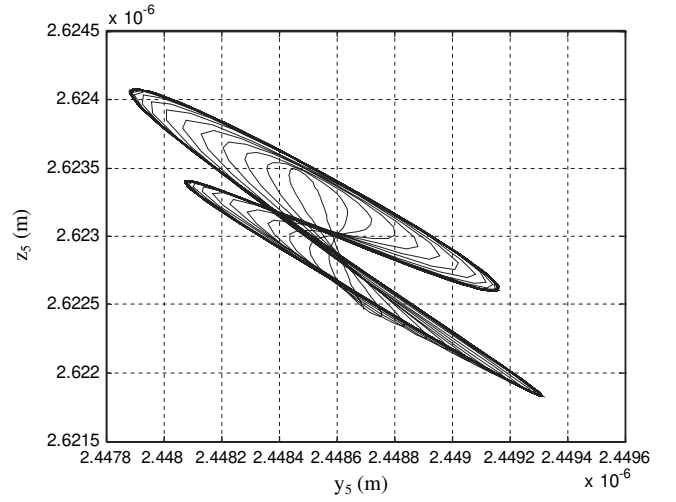


Fig. 12. Orbit plot of vibration response of the misaligned rotor in bearing 5, $\alpha_i=0.1^\circ$, AMBs with 6 magnets.

4. Analysis of the dynamic responses

Transient response is computed by solving iteratively the equations of motion (Eq. (16)) using the Newmark methods with small time increments to assure all transient dynamic changes. The steady state vibration response will be studied with and without misalignment defect. The mean of the AMB and the parameter values used in the study are listed in Table 1. The electrical and mechanical parameters values of the used electric motor in the investigated model are listed in Table 2. Fig. 6 shows time variations of the rotor angular misalignment $\alpha(t)$ and $\beta(t)$ in respectively, (x,y) and (x,z) planes. In the initials conditions, α_i , $\alpha(t)$, $\beta(t)$, $\dot{\alpha}(t)$ and $\dot{\beta}(t)$ are set to zero due to the basic assumptions in the equations of motion. It is clear that the angular time responses of $\alpha(t)$ and $\beta(t)$ takes opposite position from each others. The amplitude of the transient state motion is hasty increased as the time increases. The amplitude of oscillations reaches the steady state as time equal to 0.5 s. Fig. 7 shows the frequency response in (x,y) and (x,z) planes until 70 Hz. The horizontal axis is the frequency domain and the vertical axis is the logarithmic scale of misalignment. Curves present one dominant characteristic

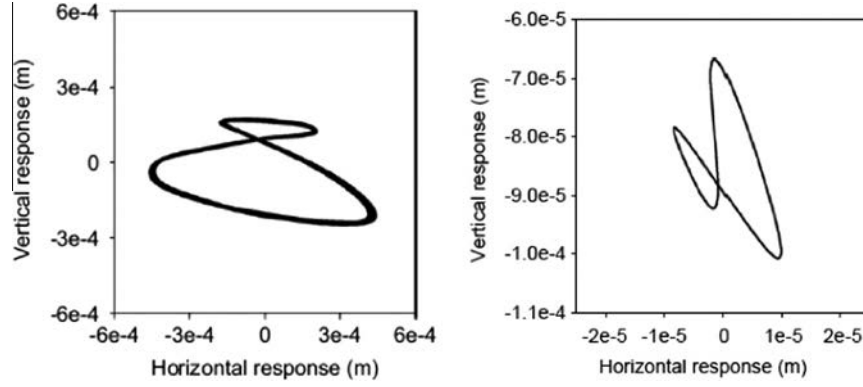


Fig. 13. Experimental orbit plot of angular misaligned rotor according to Patel and Darpe [1,22].

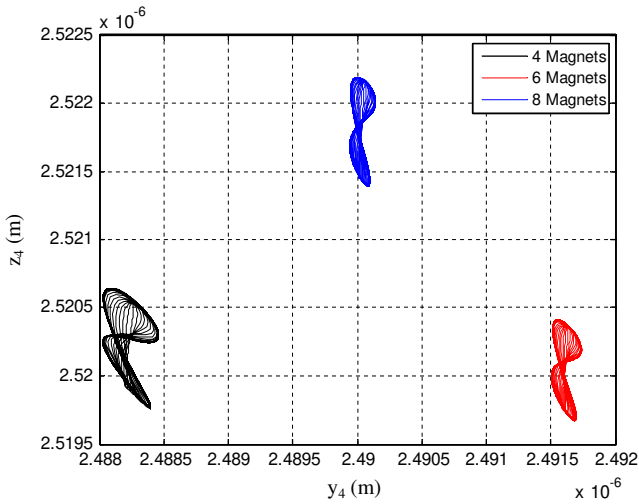


Fig. 14. Orbit plot of vibration response of the misaligned rotor in bearing 4, $\alpha_i=0.1^\circ$.

peak frequency at 44 Hz indicating the natural frequency excited at transient regime due to the presence of pure angular misalignment. Other frequencies are less important, they reflect vibrations of the transient regime. With the same starting conditions parameters, a parametric study was made to reveal the dynamic response of the investigated system with four, six and eight magnets. Figs. 8 and 9 show, respectively, temporal signal and frequencies responses, in both (x,y) and (x,z) planes, without misalignment defect. It is concluded that the decrease in the number of magnets let to intensify vibrations.

The following results are treated with the same initial conditions parameters ($\beta(t) = \dot{\alpha}(t) = \dot{\beta}(t) = 0$) but in presence of angular misalignment defect ($\alpha_i = 0.1^\circ$). Fig. 10 depicts the frequency component of the misaligned rotor in (x,y) plane. Numerical results show the presence of both lateral and torsional natural frequency excited at transient regime due to the presence of pure angular misalignment. For the chosen parameters, the torsional frequency is approximately two times the excited lateral natural frequency. The second natural frequency is not excited when the imposed angle α_i is set to zero (Fig. 7). Orbits of the driven rotor in the center of both bearings 4 and 5 are shown respectively in Figs. 11 and 12. For the chosen parameters, it can be seen that orbits have two outer loops. They are typical of those observed in the field of rotating machinery and published experimental works presented by Patel and Darpe [1,22] (Fig. 13) and Redmond [21]. These authors have concluded that, for angularly misalignment, rotors might exhibit outer looped orbits. Our results are in good agreement with exper-

imental data presented in these papers. In fact, orbits described by the centers of bearings 4 and 5 of the theoretical model developed in the present work have also two outer loops. They are due to the excitation of the lateral and torsional natural frequencies at transient regime. Fig. 14 presents the influence of the magnet's number in each bearing on the driven rotor displacement trajectories. It is assumed that orbits have less oscillations amplitudes in the case of bearing with eight pole legs. However their orientations and form still remain unchanged.

5. Conclusions

A model of rotor AMBs system was selected to exhibit one of the important defects in the field of rotating machinery. The investigated system, modeled with ten degree of freedom, was presented to allow evaluation of the correlation between shaft vibration and misalignment defect. The driving and the driven rotor were connected by a flexible coupling. The first rotor was motorized by an electric motor with a torque was expressed as a function of the shaft's angular position. The AMBs' dynamics support parameters were modeled by eight linearized stiffness and damping coefficients. Three models of AMBs were used with four, six and eight magnets were powered by bias and control currents. The global equations of motion of the driven rotor were derived and solved using the Newmark method. A numerical analysis of the spatial angular misalignment effects on the transient dynamics of the driven rotor is realized. Results have show that the lateral and torsional natural frequencies were excited at transient regime due to the presence of pure angular misalignment. Orbits of the driven rotor center had two inner loops. These were due to the excitation of the lateral and torsional natural frequencies at transient regime. This work can be extended to include parallel and combined misalignment by using co-ordinate transformation, which will be presented in future work.

Acknowledgments

The authors gratefully acknowledge Professor T.H. Patel from Charotar Institute of Technology, India and Professor A.K. Darpe from Indian Institute of Technology for their permission to use their experimental work, as in Fig. 13, to validate the numerical work presented in this paper.

Appendix A

The electromagnetic forces of AMB with four, six and eight pole legs resulting in the vertical and horizontal directions can be written, respectively, as [4]:

$$F_{y_4} = a \left[\frac{1 - \frac{k_p y}{I_0} - \frac{k_d \dot{y}}{I_0}}{1 - \frac{y}{C_0}} \right]^2 - \frac{1 + \frac{k_p y}{I_0} + \frac{k_d \dot{y}}{I_0}}{1 + \frac{y}{C_0}} \right] \quad (A1)$$

$$F_{z_4} = a \left[\frac{1 - \frac{i_0}{I_0} - \frac{k_p z}{I_0} - \frac{k_d \dot{z}}{I_0}}{1 - \frac{z}{C_0}} \right]^2 - \frac{1 + \frac{i_0}{I_0} + \frac{k_p z}{I_0} + \frac{k_d \dot{z}}{I_0}}{1 + \frac{z}{C_0}} \right] \quad (A2)$$

$$F_{y_6} = a \left[\frac{1 - \frac{k_p y}{I_0} - \frac{k_d \dot{y}}{I_0}}{1 - \frac{y}{C_0}} \right]^2 - \frac{1 + \frac{k_p y}{I_0} + \frac{k_d \dot{y}}{I_0}}{1 + \frac{y}{C_0}} \right] + \frac{a}{2} \left[\left(\frac{1 - \frac{i_0}{I_0} - \frac{k_p (y + \sqrt{3}z) + k_d (\dot{y} + \sqrt{3}\dot{z})}{2I_0}}{1 - \frac{x + \sqrt{3}z}{2C_0}} \right)^2 - \left(\frac{1 + \frac{i_0}{I_0} + \frac{k_p (y + \sqrt{3}z) + k_d (\dot{y} + \sqrt{3}\dot{z})}{2I_0}}{1 + \frac{x + \sqrt{3}z}{2C_0}} \right)^2 \right] - \frac{a}{2} \left[\left(\frac{1 - \frac{i_0}{I_0} - \frac{k_p (\sqrt{3}z - y) + k_d (\sqrt{3}\dot{z} - \dot{y})}{2I_0}}{1 - \frac{\sqrt{3}z - y}{2C_0}} \right)^2 - \left(\frac{1 + \frac{i_0}{I_0} + \frac{k_p (\sqrt{3}z - y) + k_d (\sqrt{3}\dot{z} - \dot{y})}{2I_0}}{1 + \frac{\sqrt{3}z - y}{2C_0}} \right)^2 \right] \quad (A3)$$

$$F_{z_6} = \left[\left(\frac{1 - \frac{i_0}{I_0} - \frac{k_p (y + \sqrt{3}z) + k_d (\dot{y} + \sqrt{3}\dot{z})}{2I_0}}{1 - \frac{y + \sqrt{3}z}{C_0}} \right)^2 - \left(\frac{1 + \frac{i_0}{I_0} + \frac{k_p (y + \sqrt{3}z) + k_d (\dot{y} + \sqrt{3}\dot{z})}{2I_0}}{1 + \frac{y + \sqrt{3}z}{C_0}} \right)^2 \right] + \left(\frac{1 - \frac{i_0}{I_0} - \frac{k_p (\sqrt{3}z - y) + k_d (\sqrt{3}\dot{z} - \dot{y})}{2I_0}}{1 - \frac{y + \sqrt{3}z}{C_0}} \right)^2 - \left(\frac{1 + \frac{i_0}{I_0} + \frac{k_p (\sqrt{3}z - y) + k_d (\sqrt{3}\dot{z} - \dot{y})}{2I_0}}{1 + \frac{y + \sqrt{3}z}{C_0}} \right)^2 \right] \frac{\sqrt{3}}{2} a \quad (A4)$$

$$F_{y_8} = a \left[\frac{1 - \frac{k_p y}{I_0} - \frac{k_d \dot{y}}{I_0}}{1 - \frac{y}{C_0}} \right]^2 - \frac{1 + \frac{k_p y}{I_0} + \frac{k_d \dot{y}}{I_0}}{1 + \frac{y}{C_0}} \right] + \frac{\sqrt{2}a}{2} \left[\left(\frac{1 - \frac{i_0}{I_0} - \frac{\sqrt{2}(k_p (y+z) + k_d (\dot{y} + \dot{z}))}{2I_0}}{1 - \frac{\sqrt{2}(y+z)}{2C_0}} \right)^2 - \left(\frac{1 + \frac{i_0}{I_0} + \frac{\sqrt{2}(k_p (y+z) + k_d (\dot{y} + \dot{z}))}{2I_0}}{1 + \frac{\sqrt{2}(y+z)}{2C_0}} \right)^2 \right] - \frac{\sqrt{2}a}{2} \left[\left(\frac{1 - \frac{i_0}{I_0} - \frac{\sqrt{2}(k_p (z-y) + k_d (\dot{z} - \dot{y}))}{2I_0}}{1 - \frac{\sqrt{2}(z-y)}{2C_0}} \right)^2 - \left(\frac{1 + \frac{i_0}{I_0} + \frac{\sqrt{2}(k_p (z-y) + k_d (\dot{z} - \dot{y}))}{2I_0}}{1 + \frac{\sqrt{2}(z-y)}{2C_0}} \right)^2 \right] \quad (A5)$$

$$F_{z_8} = a \left[\frac{1 - \frac{i_0}{I_0} - \frac{k_p z}{I_0} - \frac{k_d \dot{z}}{I_0}}{1 - \frac{z}{C_0}} \right]^2 - \frac{1 + \frac{i_0}{I_0} + \frac{k_p z}{I_0} + \frac{k_d \dot{z}}{I_0}}{1 + \frac{z}{C_0}} \right] + \frac{\sqrt{2}a}{2} \left[\left(\frac{1 - \frac{i_0}{I_0} - \frac{\sqrt{2}(k_p (y+z) + k_d (\dot{y} + \dot{z}))}{2I_0}}{1 - \frac{\sqrt{2}(y+z)}{2C_0}} \right)^2 - \left(\frac{1 + \frac{i_0}{I_0} + \frac{\sqrt{2}(k_p (y+z) + k_d (\dot{y} + \dot{z}))}{2I_0}}{1 + \frac{\sqrt{2}(y+z)}{2C_0}} \right)^2 \right] + \frac{\sqrt{2}a}{2} \left[\left(\frac{1 - \frac{i_0}{I_0} - \frac{\sqrt{2}(k_p (z-y) + k_d (\dot{z} - \dot{y}))}{2I_0}}{1 - \frac{\sqrt{2}(z-y)}{2C_0}} \right)^2 - \left(\frac{1 + \frac{i_0}{I_0} + \frac{\sqrt{2}(k_p (z-y) + k_d (\dot{z} - \dot{y}))}{2I_0}}{1 + \frac{\sqrt{2}(z-y)}{2C_0}} \right)^2 \right] \quad (A6)$$

where \dot{y} and \dot{z} respectively correspond to the velocities of the rotor in the y and z directions and a is the coefficient of the electromagnetic forces, it can be expressed by [4]:

$$a = \frac{\mu_0 AN^2 I_0^2}{4C_0^2} \cos\theta.$$

References

- [1] Patel Tejas H, Darpe Ashish K. Experimental investigations on vibration response of misaligned rotors. *Mech Syst Signal Process* 2009;23:2236–52.
- [2] Bouaziz S, Attia Hili M, Maatar M, Fakhfakh T, Haddar M. Dynamic behaviour of hydrodynamic journal bearings in presence of rotor spatial angular misalignment. *Mech Mach Theory* 2009;44(8):1548–59.
- [3] Attia Hili M, Bouaziz S, Maatar M, Fakhfakh T, Haddar M. Hydrodynamic and elastohydrodynamic studies of a cylindrical journal bearing. *J Hydrodyn* 2010;22(2):155–63.
- [4] Bouaziz S, Belhadj Messaoud N, Maatar M, Fakhfakh T, Haddar M. A theoretical model for analyzing the dynamic behaviour of spatially misaligned rotor with active magnetic bearings. *Mechatronics* 2011;21:899–907.
- [5] Belhadj Messaoud N, Bouaziz S, Maatar M, Fakhfakh T, Haddar M. Dynamic behaviour of active magnetic bearings in presence of angular misalignment defect. *Int J Appl Mech* 2011;3(3):491–505.
- [6] Wang KW, Lai JS. Parametric control of structural vibrations via adaptable stiffness dynamic absorbers. *ASME J Vib Acoust* 1996;118:41–7.
- [7] Mohamed AM, Emad FP. Nonlinear oscillations in magnetic bearing system. *IEEE Trans Autom Control* 1993;38:1242–5.
- [8] Attia Hili M, Bouaziz S, Maatar M, Fakhfakh T, Haddar M. Processing transient response of a flexible rotor-bearing system with unbalanced disk. *Mach Dyn Res* 2010;34(1):23–37.
- [9] Lees AW. Misalignment in rigidly coupled rotors. *J Sound Vib* 2007;305:261–71.
- [10] Dewell DL, Mitchell LD. Detection of misaligned disk coupling using spectrum analysis. *J Vib Acou Stress Reliab Des* 1984;106:9–16.
- [11] Gibbons CB. Coupling misalignment forces. In: *Proceedings of the 5th turbo machinery symposium*. Texas: Gas Turbine Laboratory, Texas A & M University; 1976. p. 111–6.
- [12] Sekhar AS, Prabhu BS. Effects of coupling misalignment on vibration of rotating machines. *J Sound Vib* 1995;185:655–71.
- [13] Lee YS, Lee CW. Modelling and analysis of misaligned rotor–ball bearing systems. *J Sound Vib* 1999;224:17–32.
- [14] Xu M, Marangoni RD. Vibration analysis of a motor-flexible coupling rotor system subject to misalignment and unbalance—part 1: theoretical model analysis. *J Sound Vib* 1994;176:663–79.
- [15] Xu M, Marangoni RD. Vibration analysis of a motor-flexible coupling rotor system subject to misalignment and unbalance—part 2: experimental validation. *J Sound Vib* 1994;176:681–91.
- [16] Al-Hussain KM, Redmond I. Dynamic response of two rotors connected by rigid mechanical coupling with parallel misalignment. *J Sound Vib* 2002;249:483–98.
- [17] Bahaloo H, Ebrahimi A, Samadi M. Misalignment modeling in rotating systems. In: *Proceedings of ASME Turbo Expo 2009: power for land, sea and air*. GT2009. Orlando, FL, USA; June 8–12, 2009. paper GT2009-60121;1–7.
- [18] Zhang W, Zu JW. Transient and steady non-linear response for a rotor-active magnetic bearings system with time-varying stiffness. *Chaos Solitons Fract* 2008;38:1152–67.
- [19] Khabou MT, Bouchaala N, Chaari F, Fakhfakh T, Haddar M. Study of a spur gear dynamic behavior in transient regime. *Mech Syst Signal Process* 2011;25:3089–101.
- [20] Preve C, Jeannot R. *Guide de Conception Des Réseaux Électriques Industriels*. DAS Transport et distribution, Schneider Electric; 1997.
- [21] Redmond I. Study of a misaligned flexibly coupled shaft system having non-linear bearings and cyclic coupling stiffness—Theoretical model and analysis. *J Sound Vib* 2010;329:700–20.
- [22] Patel Tejas H, Darpe Ashish K. Vibration response of misaligned rotors. *J Sound Vib* 2009;325:609–28.